Nuclear Modification of Quarkonium Production in p+Pb Collisions at the LHC

R. Vogt

Physics Division, Lawrence Livermore National Laboratory, Livermore, CA 94551, USA

Physics Department, University of California, Davis, CA 95616, USA

J/ψ and Υ Production in $\sqrt{s_{NN}} = 5$ TeV p+Pb Collisions

- **Production of open $Q\overline{Q}$ and quarkonium in pp**
- **Calculations of $R_{p\mathrm{Pb}}(p_T)$ at forward, backward and midrapidity, $R_{p\mathrm{Pb}}(y)$, and forward/backward ratios $R_{FB}(p_T)$ and $R_{FB}(y)$**
  - **Dependence of ratios on proton PDF**
  - **EPS09 with uncertainties**
  - **LO vs NLO, EPS09 and nDS(g)**
  - **Central EPS09 compared to nDS, nDSg and EKS98**
- **Factorization of cold matter effects: R_{PbPb} vs $R_{p\mathrm{Pb}} \times R_{\mathrm{Pb}p}$**

J/ψ Calculation in NLO CEM Based on Fitting $\sigma_{c\bar{c}}$

Caveat: full NNLO cross section unknown, could still be large corrections

Employ $m = 1.27$ GeV, lattice value at $m(3\,\mathrm{GeV})$ and use subset of $c\bar{c}$ total cross section data to fix μ_F/m $(2.1^{+2.55}_{-0.85})$ and μ_R/m $(1.6^{+0.11}_{-0.12})$ with CT10 PDFs

Result with $\Delta\chi^2 = 1$ gives uncertainty on scale parameters; $\Delta\chi^2 = 2.3$ gives one standard deviation on total cross section, expect results on $b\bar{b}$ and Υ soon

LHC $pp \to c\bar{c}$ at $\sqrt{s} = 7$ TeV not included but agrees well

The $c\bar{c}$ mass and scale parameters are used to calculate J/ψ

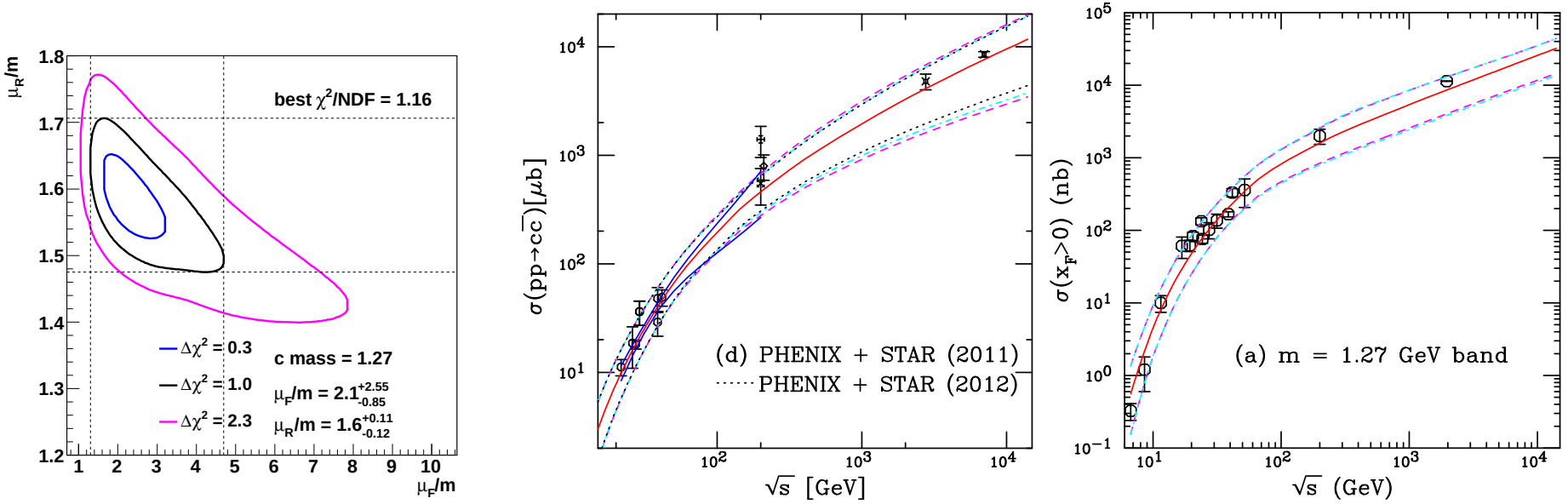

Figure 1: (Left) The χ^2/dof contours for fits including the STAR 2011 cross section but excluding the STAR 2004 cross section. The best fit values are given for the furthest extent of the $\Delta\chi^2 = 1$ contours. (Center) The energy dependence of the charm total cross section compared to data. The best fit values are given for the furthest extent of the $\Delta\chi^2 = 1$ contours. The central value of the fit in each case is given by the solid red curve while the dashed magenta curves and dot-dashed cyan curves show the extent of the corresponding uncertainty bands. The dashed curves outline the most extreme limits of the band. In addition, the dotted black curves show the uncertainty bands obtained with the 2012 STAR results while the solid blue curves in the range $19.4 \le \sqrt{s} \le 200$ GeV represent the uncertainty obtained from the extent of the $\Delta\chi^2 = 2.3$ contour. (Right) The uncertainty band on the forward J/ψ cross section. The dashed magenta curves and dot-dashed cyan curves show the extent of the corresponding uncertainty bands. The dashed curves outline the most extreme limits of the band. (RV, R Nelson and A D Frawley, Phys. Rev. C **87** (2013) 014908.)

Results on LHC Charm Distributions

Excellent agreement with $\sqrt{s} = 7$ TeV ALICE pp data on muons in the forward region $(2.5 < y < 4)$

Leptons from semi-leptonic heavy flavor decays include contributions from $D \to \mu X$, $B \to \mu X$, $B \to D \to \mu X$, all with $\sim 10\%$ decay branching ratios

Fit results gives narrower uncertainty without reducing agreement with data than fiducial results based on $m = 1.5$ GeV

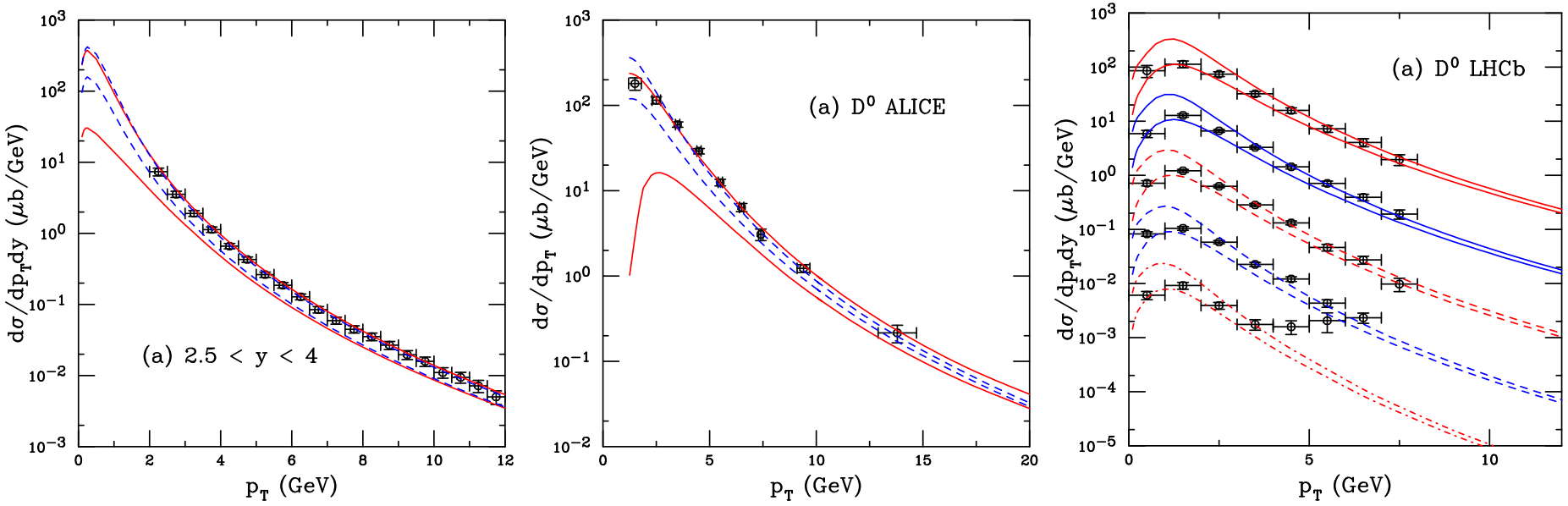

Figure 2: (Left) Comparison of the single lepton p_T distributions in the rapidity interval $2.5 < y < 4$ at $\sqrt{s} = 7$ TeV calculated with the FONLL set for charm (solid red) and the fitted set with $m = 1.27$ GeV (dashed black). (Center) Our calculations are compared with the reconstructed ALICE D^0 data in $|y| \leq 0.5$. The FONLL uncertainty bands with the fiducial charm parameter set are shown by the red solid curves while the blue dashed curves are calculated with the charm fit parameters. (Right) Our calculations are compared with the reconstructed LHCb D^0 data in the rapidity intervals: $2 < y < 2.5$ (solid red); $2.5 < y < 3$ (solid blue); $3 < y < 3.5$ (dashed red); $3.5 < y < 4$ (dashed blue); and $4 < y < 4.5$ (dot-dashed red). The rapidity intervals are separated by a factor of 10 to facilitate comparison. The lowest rapidity interval, $2 < y < 2.5$, is not scaled. (RV, R Nelson and A D Frawley, Phys. Rev. C **87** (2013) 014908.)

Comparison to ALICE J/ψ pp Distributions

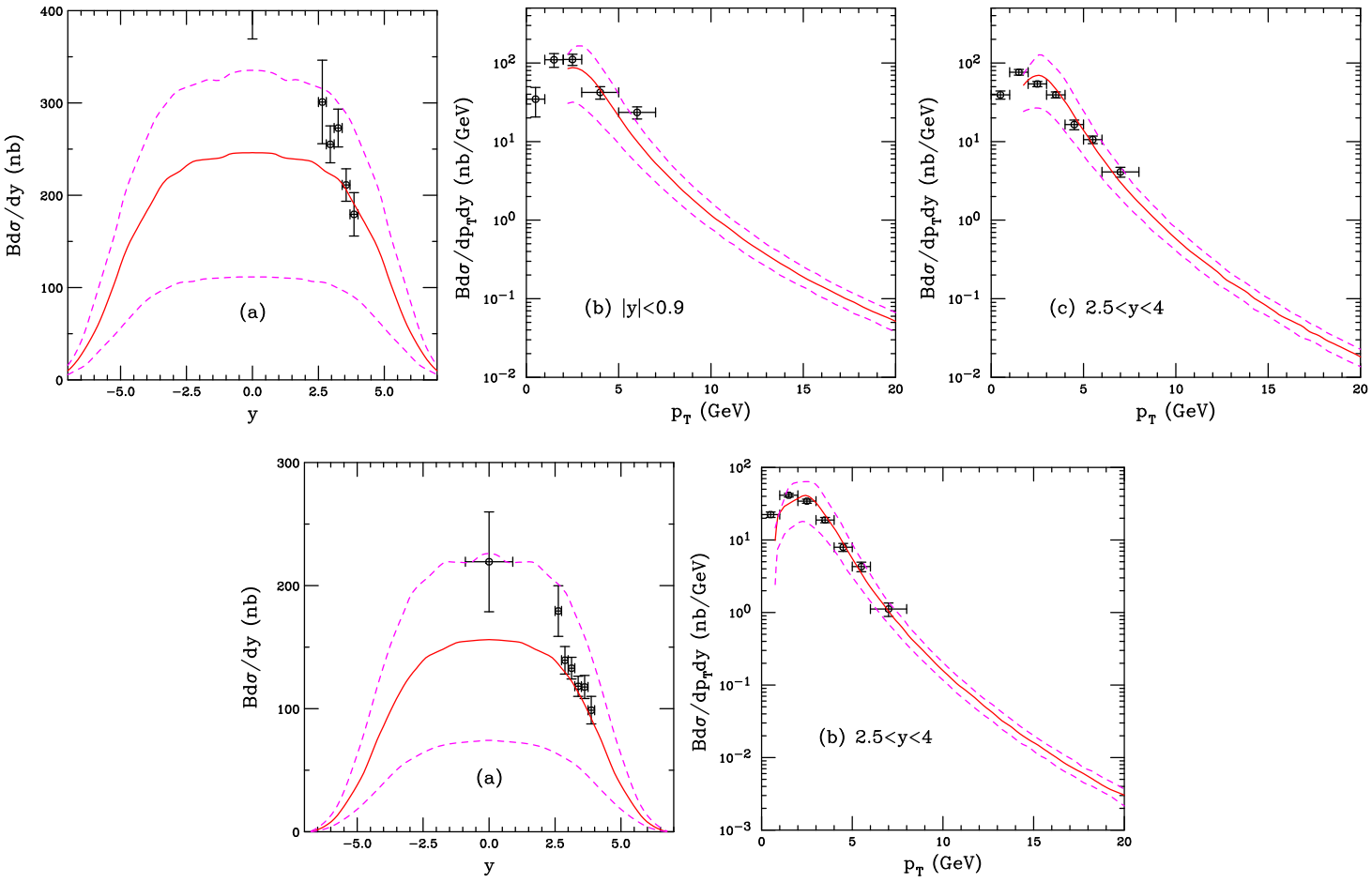

Figure 3: The J/ψ rapidity distribution (a) and the midrapidity, $|y| < 0.9$ (b), and forward rapidity, $2.5 < y < 4$ (c) p_T distributions at $\sqrt{s} = 7$ TeV (top) and 2.76 TeV (bottom) and their uncertainties. The results are compared to the ALICE rapidity distribution as well as the p_T distributions. The solid red curve shows the central value while the dashed magenta curves outline the uncertainty band. A $\langle k_T^2 \rangle$ kick of 1.49 GeV^2 is applied to the p_T distributions, as discussed in the text. (RV, R Nelson and A D Frawley, Phys. Rev. C **87** (2013) 014908.)

Υ Calculation in NLO CEM Based on Fitting $\sigma_{b\bar{b}}$

Caveat: full NNLO cross section unknown, could still be large corrections

Employ $m = 4.65$ GeV and use $b\bar{b}$ total cross section data to fix μ_F/m $(1.4^{+0.75}_{-0.47})$ and μ_R/m $(1.1^{+0.26}_{-0.19})$ with CT10 PDFs

Result with $\Delta\chi^2 = 1$ gives uncertainty on scale parameters; $\Delta\chi^2 = 2.3$ gives one standard deviation on total cross section

LHC $pp \to b\bar{b}$ at $\sqrt{s} = 7$ TeV included in fits, not enough reliable data at fixed target to help constrain

The $b\bar{b}$ mass and scale parameters are used to calculate Υ

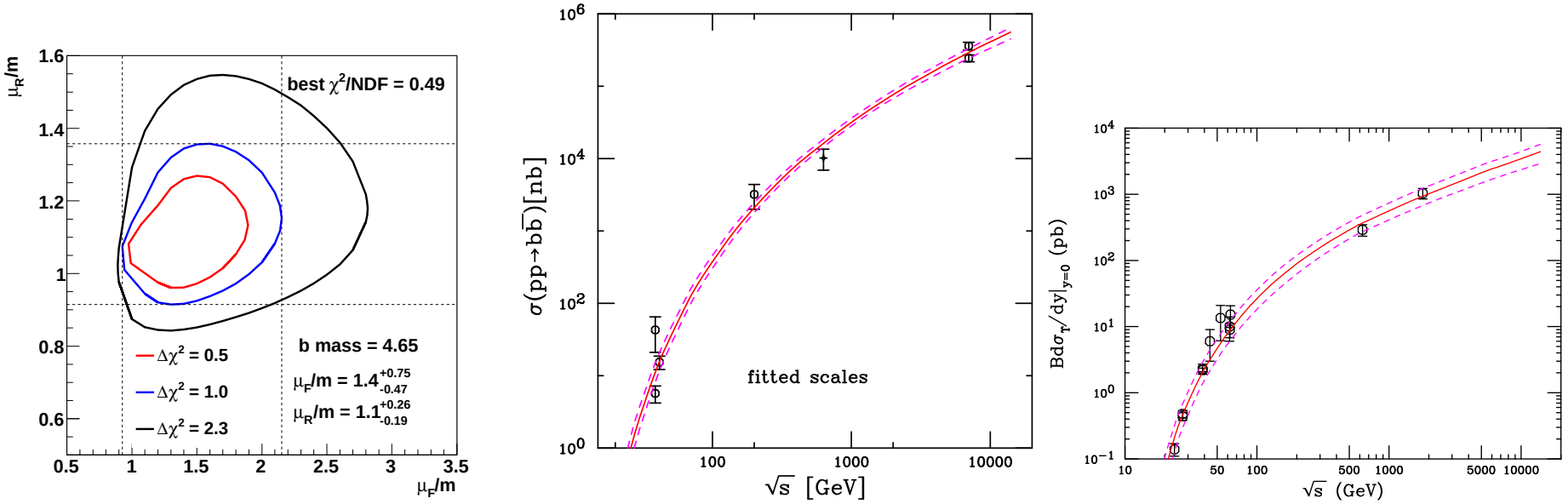

Figure 4: (Left) The χ^2/dof contours for fits. The best fit values are given for the furthest extent of the $\Delta\chi^2 = 1$ contours. (Center) The energy dependence of the bottom total cross section compared to data. The best fit values are given for the furthest extent of the $\Delta\chi^2 = 1$ contours. The central value of the fit in each case is given by the solid red curve while the dashed magenta curves show the corresponding uncertainty bands. (Right) The uncertainty band on the Υ cross section at $y = 0$. The dashed magenta curves show the extent of the corresponding uncertainty bands. (RV, R Nelson and A D Frawley, in progress)

Results for Bottom Distributions at the LHC

Good agreement with ALICE inclusive single muon distributions (left) with calculations based on charm and bottom fits

Both B hadron (center) and muons from b decays (right) show agreement with the p_T distributions

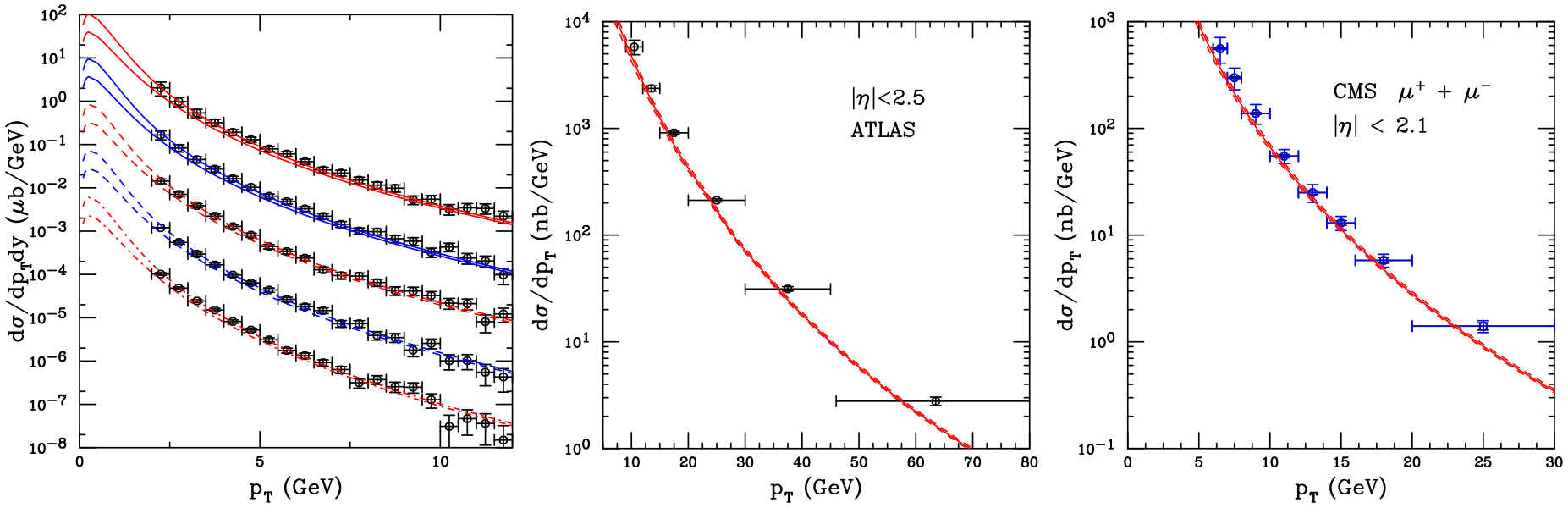

Figure 5: (Left) The ALICE inclusive single muon data from heavy flavor decays at $\sqrt{s} = 7$ TeV divided into rapidity bins, from top to bottom: $2.5 < y < 2.8$ (solid red); $2.8 < y < 3.1$ (solid blue); $3.1 < y < 3.4$ (dashed red); $3.4 < y < 3.7$ (dashed blue); and $3.7 < y < 4$ (dot-dashed red). The top curves are shown at their calculated value, the others are scaled down by successive factors of 10 to separate them. (Center) The B hadron p_T distribution measured by ATLAS. (Right) The muon p_T distribution from b decays measured by CMS. The calculations are with the central fit set and the one standard deviation in mass and scale values. (RV, R Nelson and A D Frawley, in progress)

Comparison to $p\overline{p}$ and pp Υ Data

Need a larger broadening for the higher mass b quarks

Good agreement with Tevatron Run II data, both in the full rapidity range and separated into different rapidity regions

Agreement with CMS Υ data for $p_T < 30$ GeV, very high p_T hard to reproduce, requires high p_T resummation for logs of large p_T/m

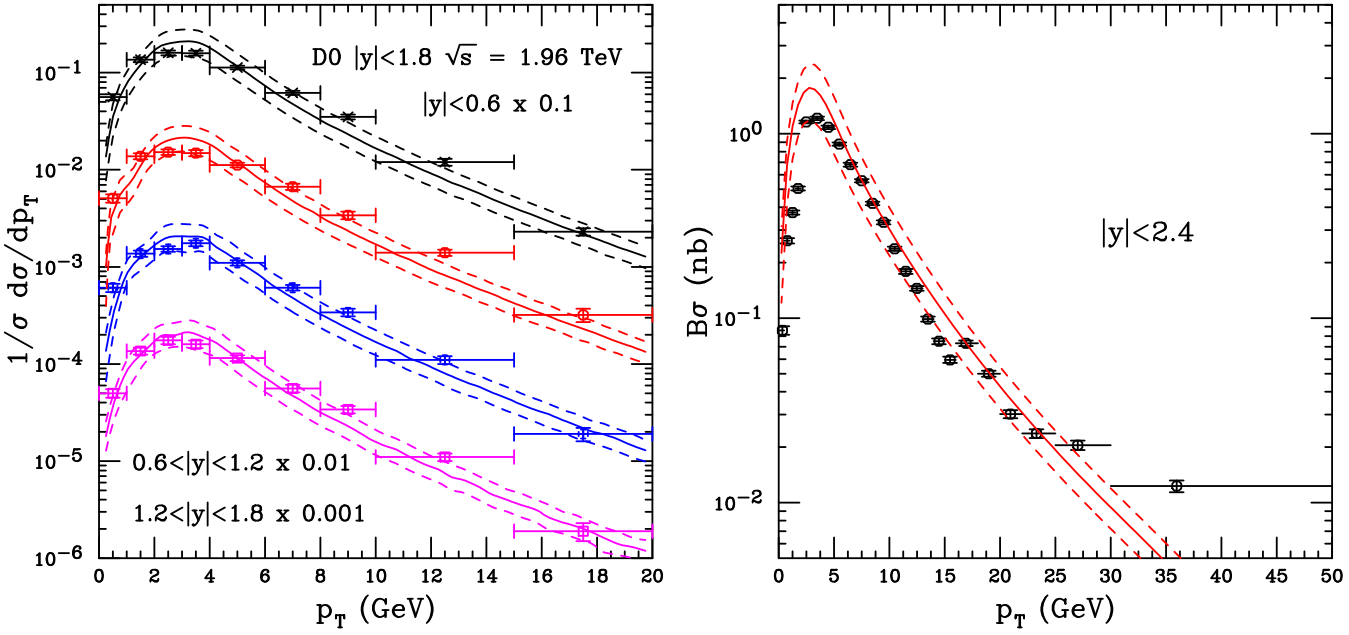

Figure 6: (Left) $\Upsilon(1S)$ p_T distribution in the full measured rapidity range, $|y| < 1.8$ (black), and different rapidity bins: $|y| < 0.8$ (red); $0.8 < |y| < 1.2$ (blue); and $1.2 < |y| < 1.8$ (magenta). The data are from the D0 collaboration with $\sqrt{s} = 1.96$ TeV in $\overline{p}p$ collisions at the Tevatron. (Right) Calculation of the $\Upsilon(1S)$ p_T distribution in pp collisions at $\sqrt{s} = 7$ TeV. The data are from the CMS collaboration and are from the rapidity range $|y| < 2.4$. (RV, R Nelson and A D Frawley, in progress)

Cold Nuclear Matter Effects in Hadroproduction

In heavy-ion collisions, one has to fold in cold matter effects, typically studied in pA or dA interactions from fixed-target energies to colliders

Hard probes, where production is calculable in QCD, are best to study differences between initial and final state effects

Important cold nuclear matter effects in hadroproduction include:

- **Initial-state nuclear effects on the parton densities (nPDFs)**
- **Initial- (or final-) state energy loss**
- **Final-state absorption on nucleons**
- **Final-state break up by comovers (hadrons or partons)**
- **Intrinsic $Q\overline{Q}$ pairs**

In this talk, I will concentrate on nuclear parton densities, not including any other effect

Nuclear PDFs at NLO

Gluon shadowing ratios compared at the J/ψ and Υ production scales

EPS09 NLO (black) and EKS98 LO (magenta) very similar for $x > 0.002$, significant antishadowing, nDS NLO (blue) and nDSg NLO (red) have almost no antishadowing, nDSg and EKS98 have stronger shadowing than central EPS09 at low x

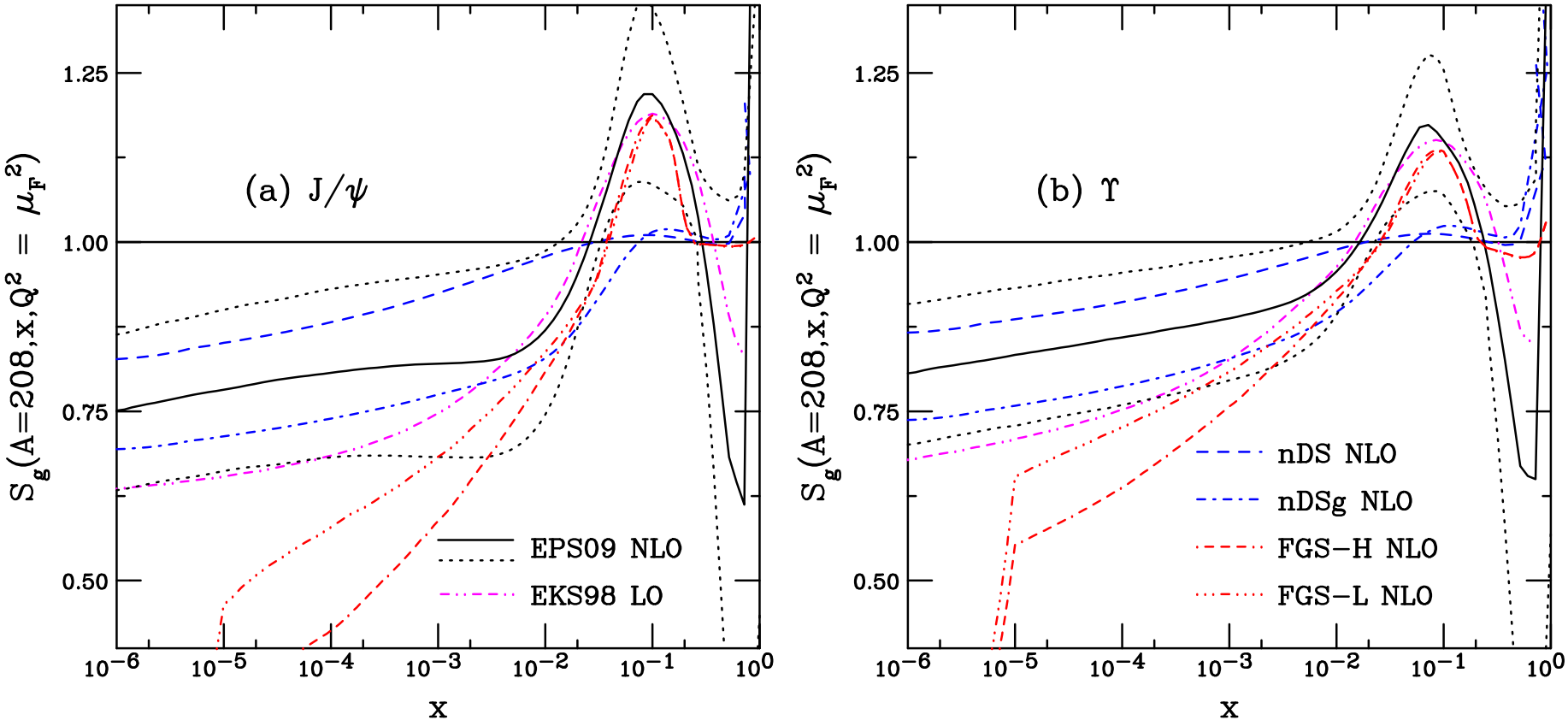

Figure 7: **Gluon shadowing ratios calculated for Pb nuclei ($A = 208$) calculated at the central value of the fitted factorization scales for J/psi (left) and Υ (right). EPS09 NLO is shown by the black solid curve while the uncertainty band is outlined by the black dotted curves. The NLO nDS and nDSg parameterizations are given in the blue dashed and red dot dashed curves. The LO EKS98 parameterization is in magenta (dot-dot-dot-dash-dashed).**

EPS09 Central Ratio Independent of Proton PDF

Even though global fit for EPS09 is based on a specific proton PDF set, the calculated shadowing ratios are basically unchanged by the choice of proton PDF

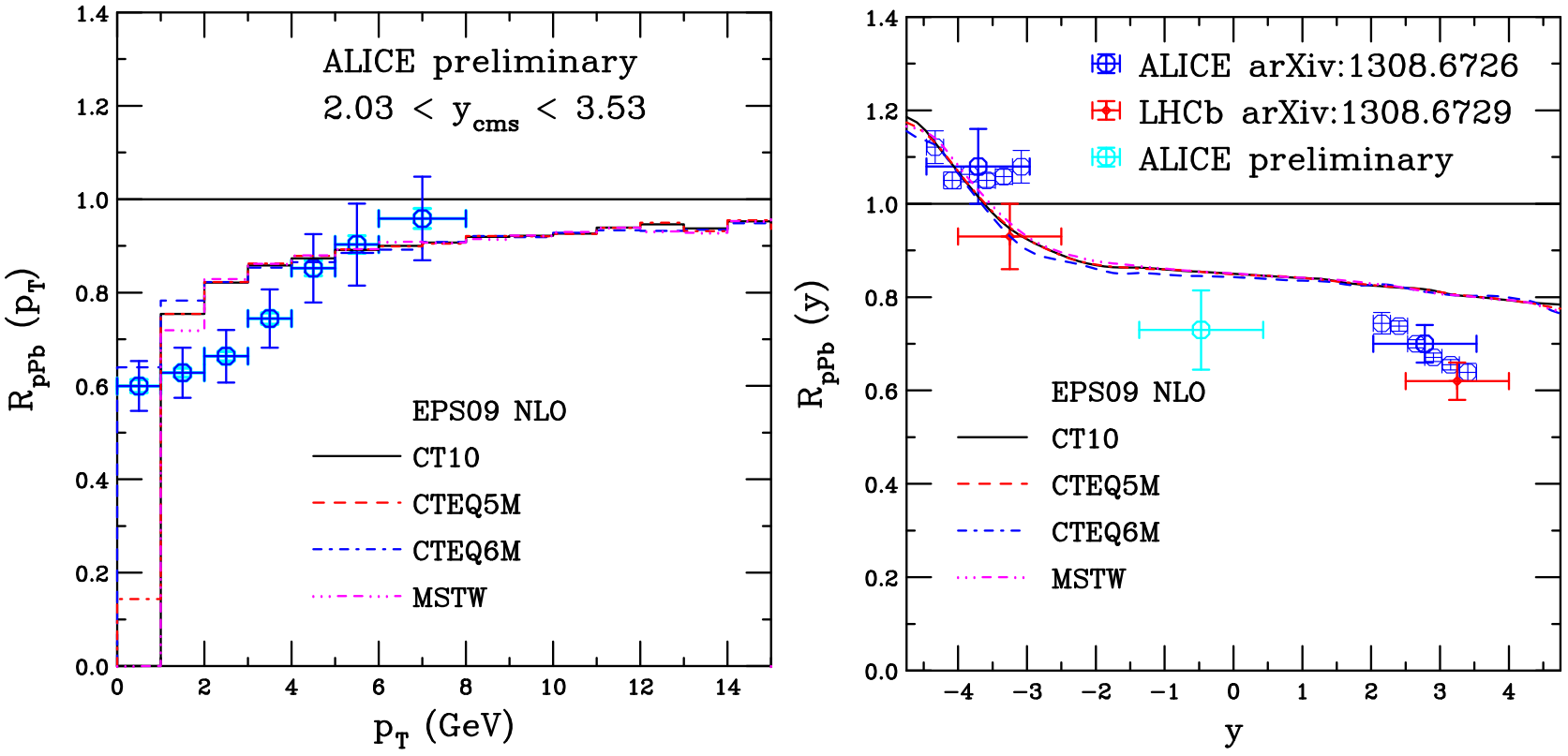

Figure 8: **The ratio $R_{p\mathrm{Pb}}(p_T)$ for ALICE at forward rapidity (left) and p_T-integrated as a function of rapidity. The ratios are for CT10 (black), nDS (blue), nDSg (red) and EKS98 (magenta).**

Calculating nPDF Uncertainties in pA

EPS09 LO and EPS09 NLO based on CTEQ61L and CTEQ6M respectively

The gluon densities in these two sets differ significantly at low x, hence the low x modifications of EPS09 LO and NLO are quite different

nPDF uncertainties calculated with the 30+1 sets of EPS09: one central set and 30 sets obtained by varying each of the 15 parameters, i.e. sets 2 and 3 were obtained by changing parameter 1 by $\pm 1\sigma_1$ *etc.* where σ_i is the standard deviation of parameter i

Uncertainties due to shadowing calculated using 30+1 error sets of EPS09 NLO added in quadrature so the uncertainty is cumulative

EPS09 Uncertainty Bands I: $R_{p\mathrm{Pb}}(p_T)$

Data typically show stronger effect than central EPS09 result alone but the data tend to fall within the uncertainty band

These calculations (also for the rapidity dependence, next slide) differ somewhat from previous results shown – the wrong scale was being passed to the nPDFs

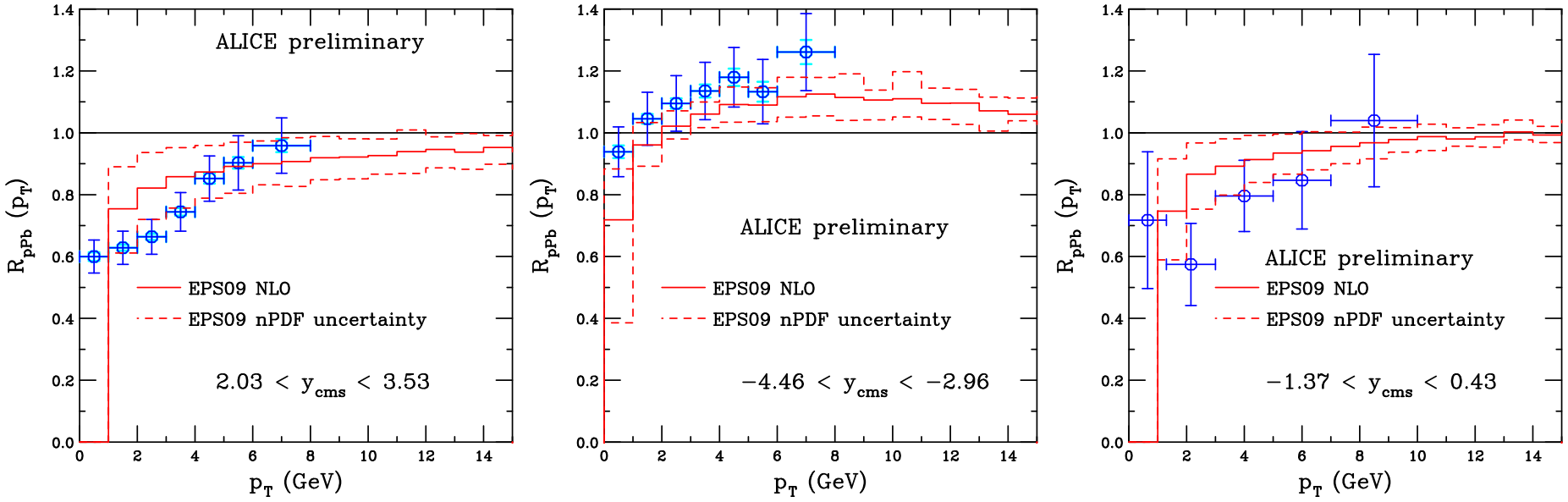

Figure 9: **The ratio $R_{p\mathrm{Pb}}(p_T)$ for ALICE at forward rapidity (left) and backward (middle) and central (right) rapidity. The EPS09 uncertainty band is shown.**

EPS09 Uncertainty Bands II: $R_{p\mathrm{Pb}}(y)$

Backward rapidity data agree with the rise at $y < -2.5$ from antishadowing onset

Preliminary midrapidity point is on the lower edge of the uncertainty band

Forward rapidity data are underestimated, only the lower edge of the uncertainty band (strongest shadowing) is consistent with data

For $y > -2.5$, the band is relatively wide, about $\pm 12\%$, and $R_{p\mathrm{Pb}}$ decreases by less than 10% in this region

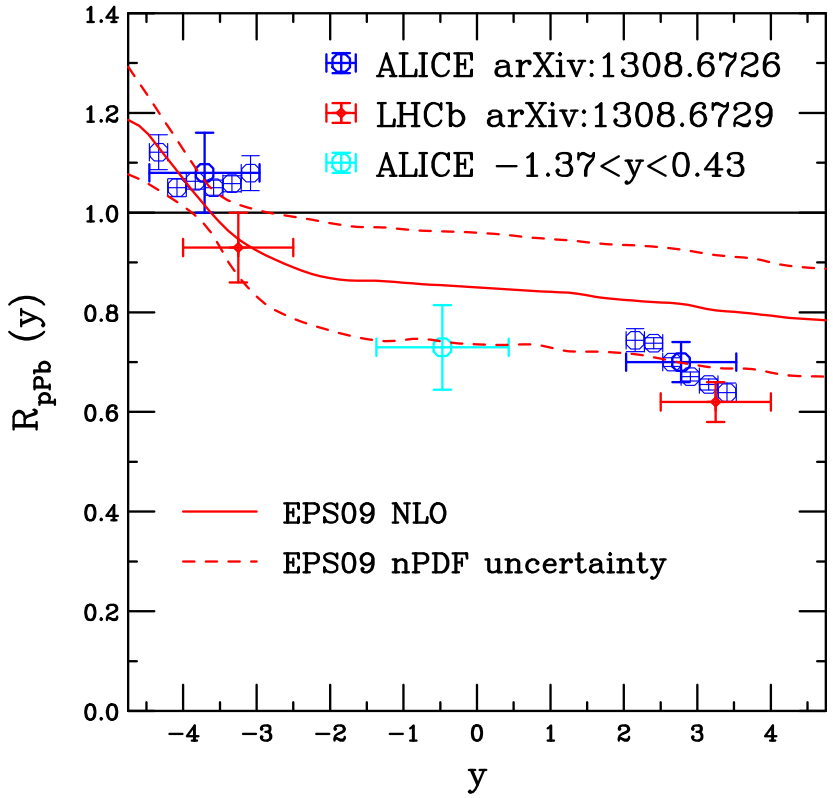

Figure 10: **The EPS09 NLO uncertainty band, $R_{p\mathrm{Pb}}(y)$.**

EPS09 Uncertainty Bands III: R_{FB}

Reduced uncertainties in the forward/backward ratio because we take the ratio before adding differences in quadrature

The p_T ratio almost flat and above the data for $p_T < 6$ GeV

Curvature of rapidity ratio at $y > 2.5$ reflects the antishadowing rise at backward rapidity and the narrower uncertainty band in this region relative to the forward region

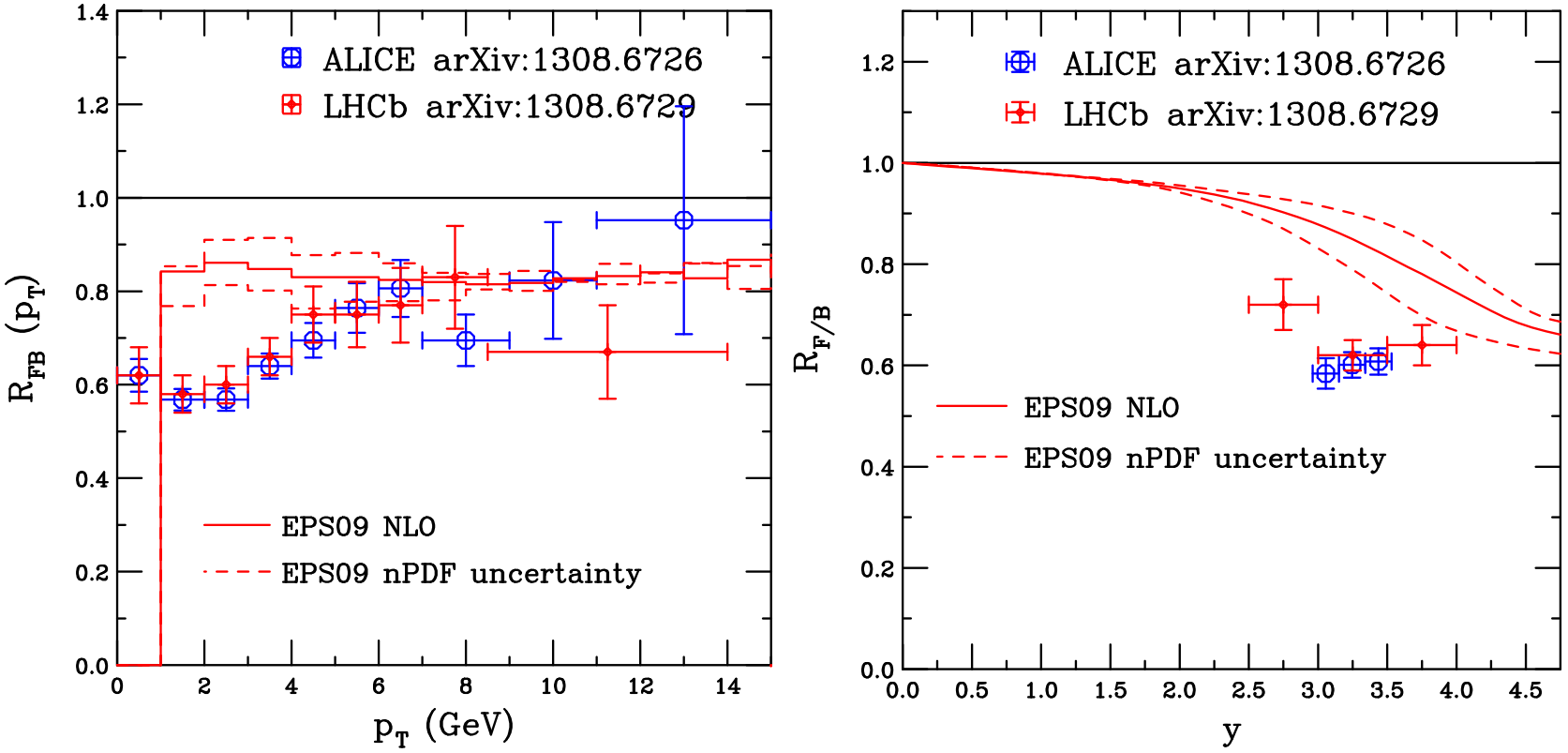

Figure 11: **The ratio $R_{p\mathrm{Pb}}(p_T)$ for ALICE at forward rapidity (left) and p_T-integrated as a function of rapidity (right). The EPS09 uncertainty band is shown.**

NLO vs LO EPS09

The nPDF set should be appropriate to the order of the calculation: if using the LO set in a NLO calculation agrees better with the data, it isn't really better

NLO calculation required for CEM to obtain p_T distribution and is, anyway, more appropriate

LO CEM uncertainty band is broader, with stronger shadowing, to counterbalance the flatter low x behavior of CTEQ61L while CTEQ6M is valence-like: different behavior of proton PDFs makes good order-by-order agreement of $R_{p\mathrm{Pb}}$ difficult

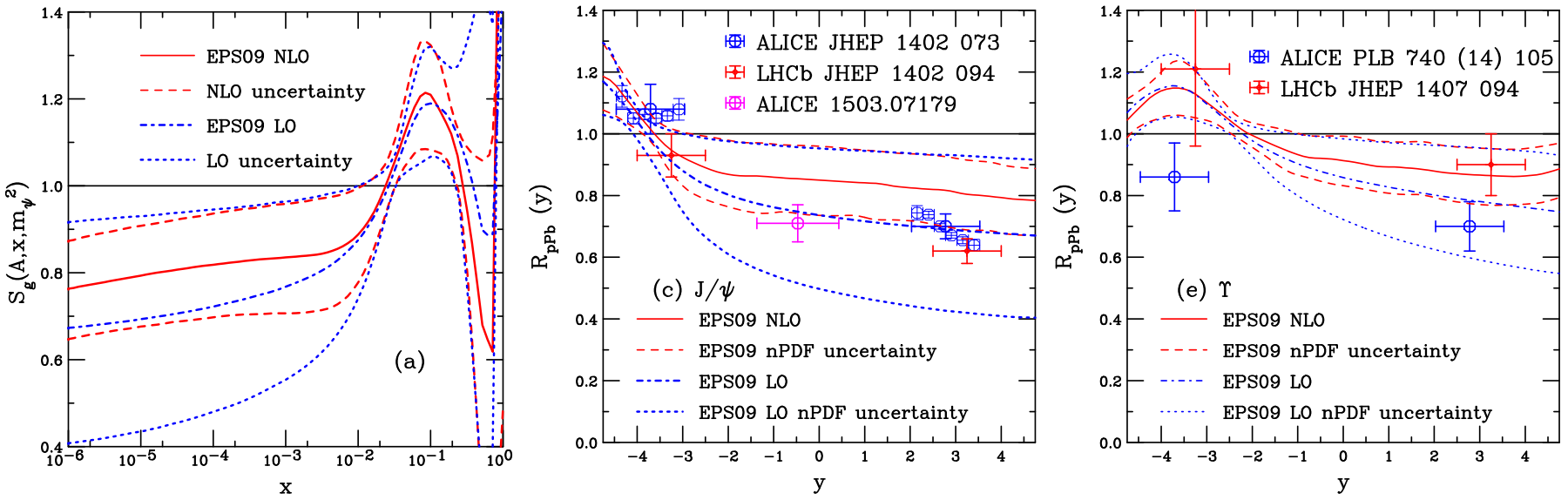

Figure 12: **(Left) The EPS09 LO (blue) and NLO (red) uncertainty bands for gluon shadowing. The corresponding uncertainty bands for $R_{p\mathrm{Pb}}(y)$ at $\sqrt{s_{NN}} = 5$ TeV for J/ψ (center) and Υ (right).**

NLO vs LO nDS

While there are some differences between the LO and NLO nDS and nDSg ratios, especially for nDSg at $x \sim 0.01$, the LO and NLO ratios are much closer than those of the EPS09 central sets, here order of calculation is not an issue

nDS(g) employs GRV98 LO and NLO proton PDFs, the Q^2 range of the nPDF, $1 < Q^2 < 10^6$ GeV^2, is above the minimum scale of GRV98, unlike EPS09 and CTEQ6

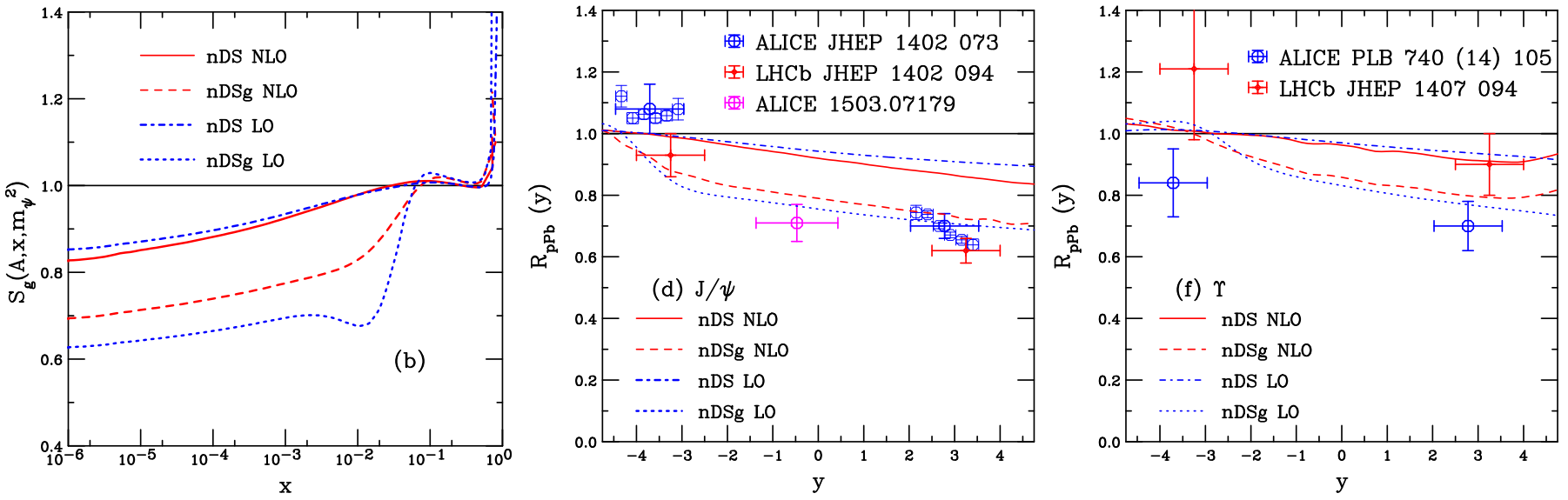

Figure 13: **(Left) The nDS and nDSg LO (blue) and NLO (red) gluon shadowing ratios. The corresponding results for $R_{p\mathrm{Pb}}(y)$ at $\sqrt{s_{NN}} = 5$ TeV are shown for J/ψ (center) and Υ (right).**

EPS09 vs Other nPDFs I: $R_{p\mathrm{Pb}}(p_T)$

Central EPS09 NLO set compared to nDS NLO, nDSg NLO and EKS98 (LO)

nDS effect is weakest of all while nDSg is weak at backward rapidity but stronger than EPS09 at mid- and forward rapidity

EKS98 and EPS09 NLO are very similar for $x > 0.01$ so they agree well at backward and mid-rapidity while EKS98 is stronger at forward rapidity

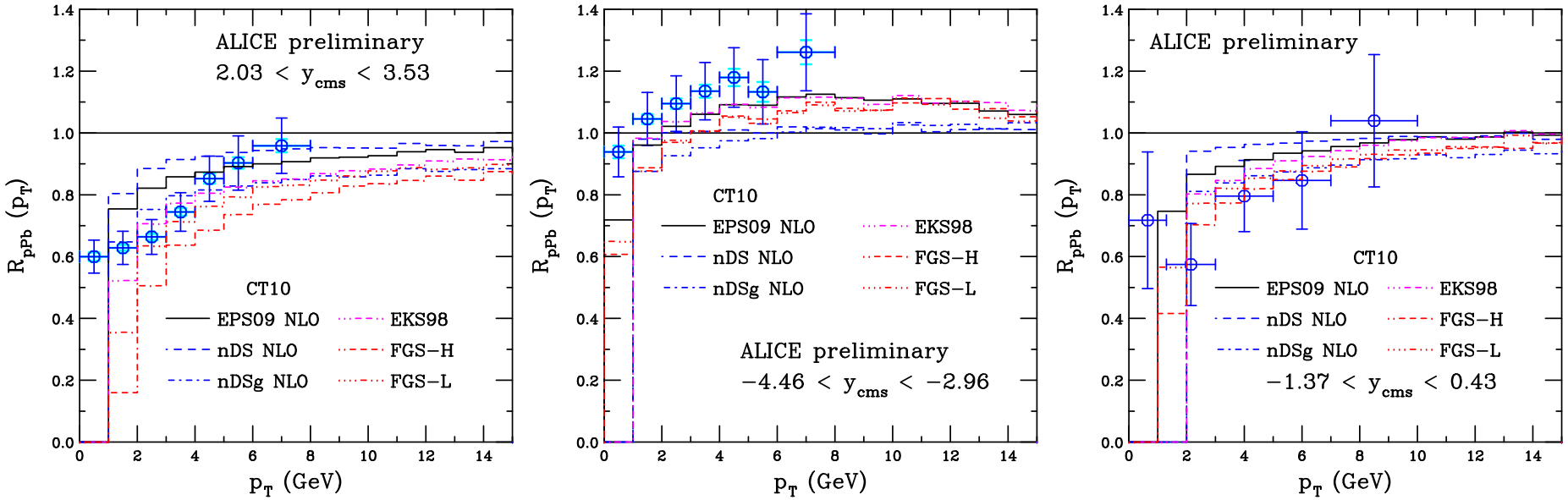

Figure 14: **The ratio $R_{p\mathrm{Pb}}(p_T)$ for ALICE at forward (left), backward (center) and mid- (right) rapidity. The ratios are for central EPS09 NLO (black), nDS NLO (blue), nDSg NLO (red) and EKS98 LO (magenta).**

EPS09 vs Other nPDFs II: $R_{p\mathrm{Pb}}(y)$

EKS98 LO follows EPS09 NLO central set until $y > -2$ where it decreases linearly while EPS09 becomes flatter

EPS09 abrupt change of slope near antishadowing region follows from the gluon shadowing ratio, almost like the low x behavior had to join to assumed antishadowing shape at intermediate x

nDS and nDSg, with no antishadowing, have a weaker y dependence overall

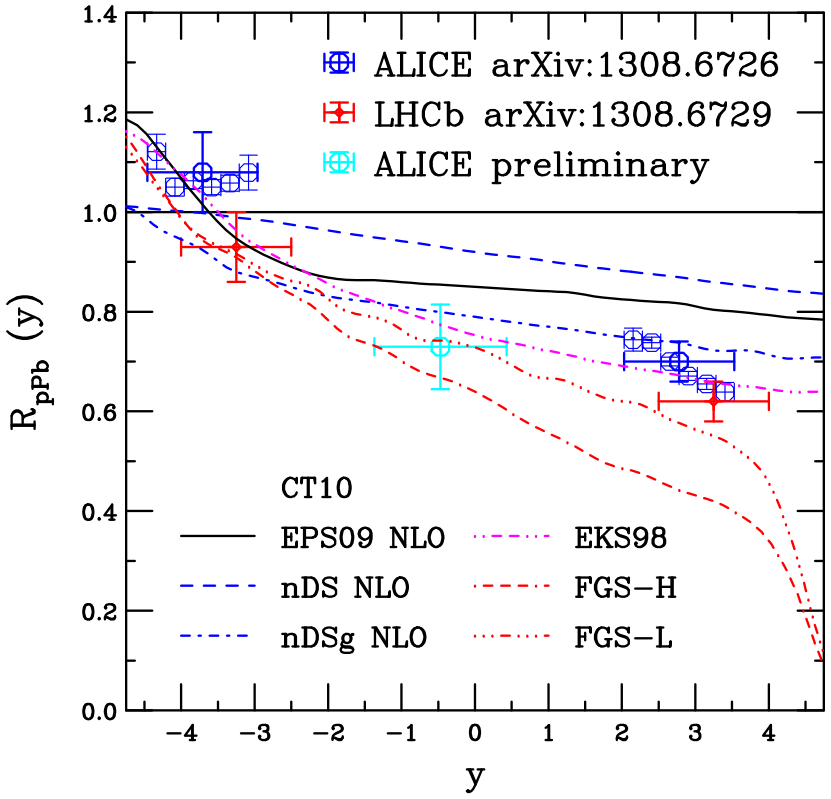

Figure 15: **The calculated $R_{p\mathrm{Pb}}(y)$ for central EPS09 NLO (black), nDS NLO (blue), nDSg NLO (red) and EKS98 LO (magenta).**

EPS09 vs Other nPDFs III: R_{FB}

nDS has strongest p_T dependence of $R_{FB}(p_T)$, EKS98 comes closest to agreement with low p_T data due to the stronger effect at low x than EPS09

Only EPS09 shows curvature in $R_{FB}(y)$, the others show an almost linear y dependence

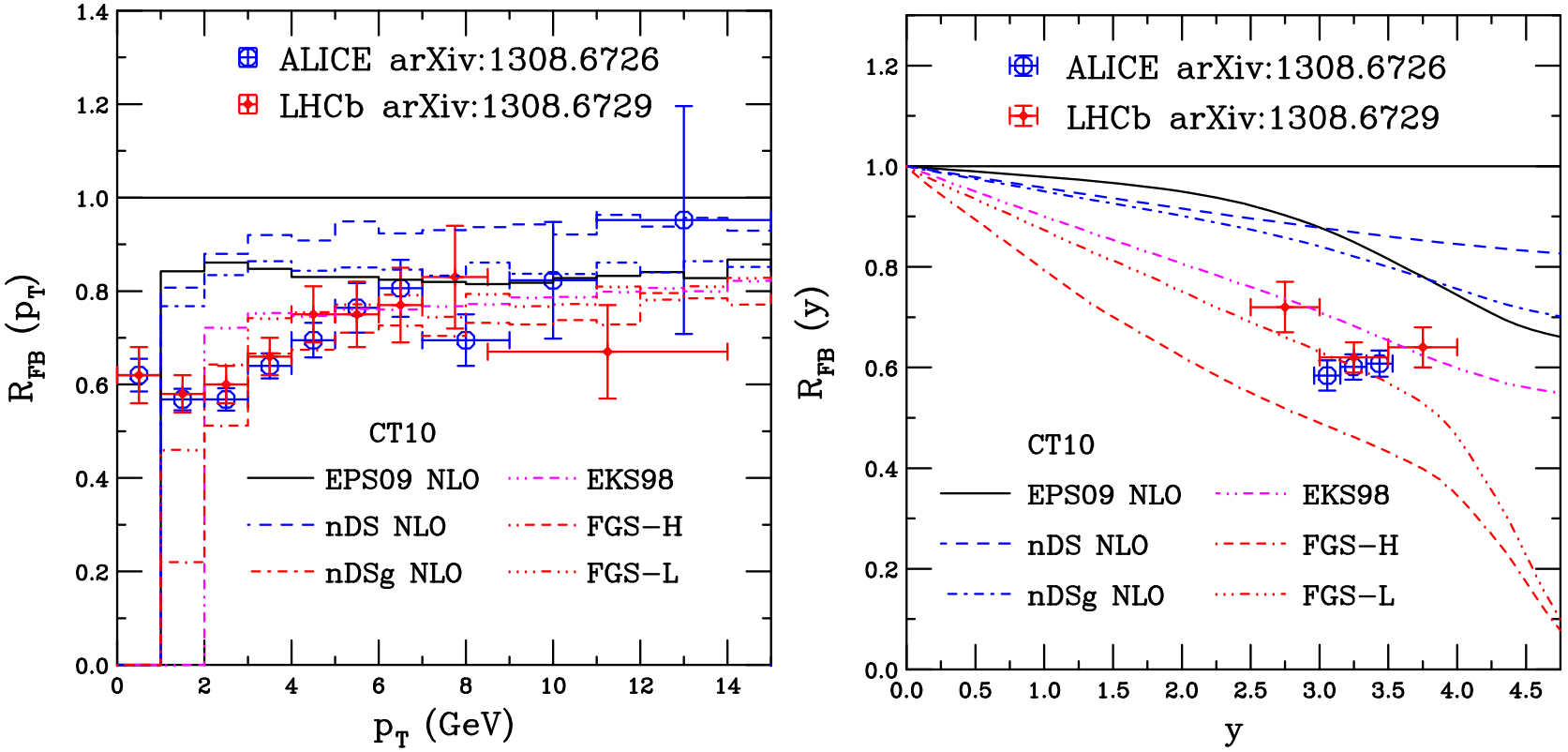

Figure 16: **The ratio $R_{p\mathrm{Pb}}(p_T)$ for ALICE at forward rapidity (left) and p_T-integrated as a function of rapidity. The ratios are for central EPS09 NLO (black), nDS NLO (blue), nDSg NLO (red) and EKS98 LO (magenta).**

EPS09 vs Other nPDFs IV: Υ $R_{p\mathrm{Pb}}(y)$, $R_{FB}(y)$

Generally relatively good agreement with $R_{p\mathrm{Pb}}$

Rather narrow antishadowing band for FGS sets

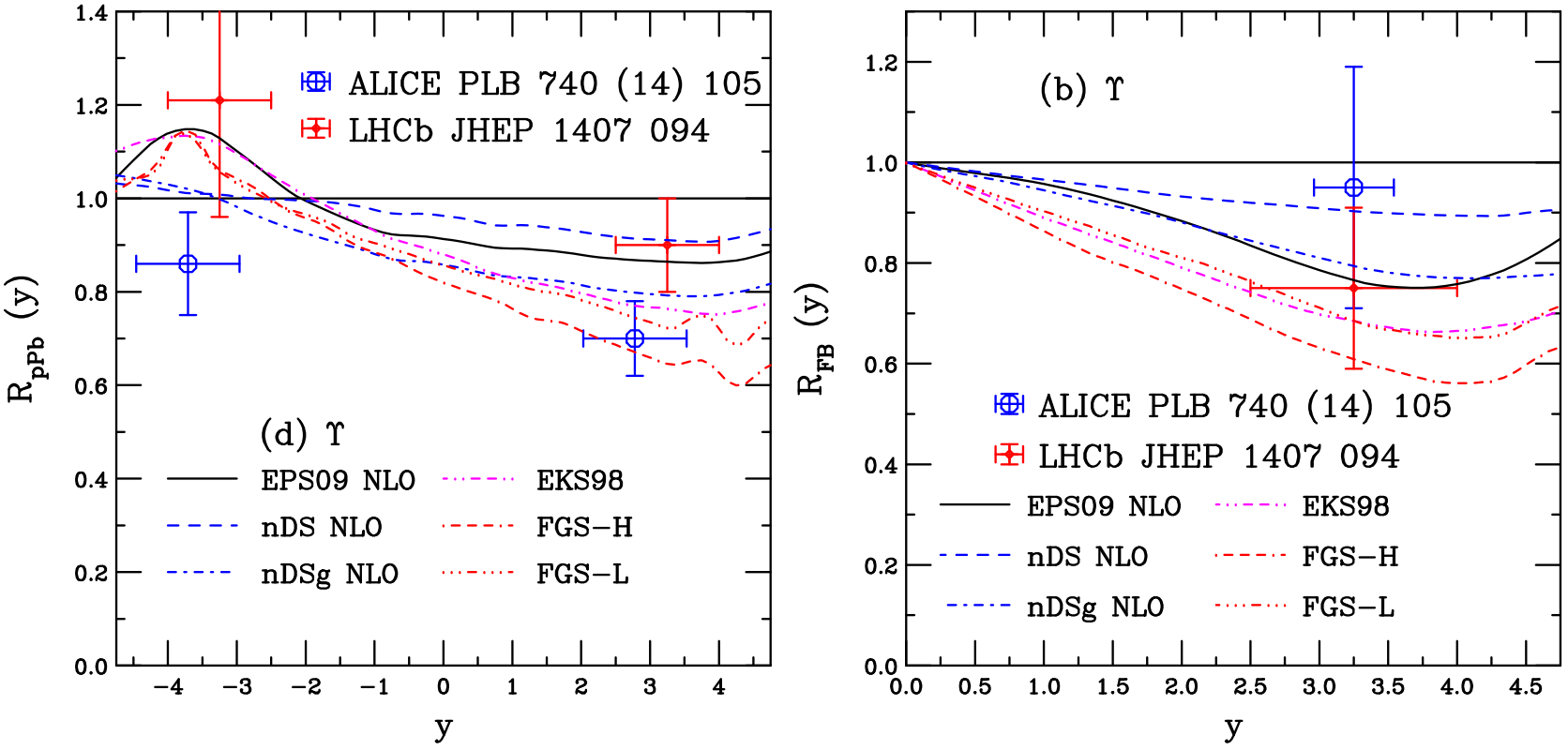

Figure 17: **The ratio $R_{p\mathrm{Pb}}(y)$ for ALICE at forward rapidity (left) and p_T-integrated as a function of rapidity. The ratios are for central EPS09 NLO (black), nDS NLO (blue dashed), nDSg NLO (blue dot dashed), EKS98 LO (magenta), FGS-H NLO (red dot-dash-dash-dashed) and FGS-L NLO (red dot-dot-dot-dashed).**

Factorization of R_{AA} into $R_{pA}(+y) \times R_{pA}(-y)$? J/ψ

The factorization is exact for the CEM at LO because the process is $2 \to 1$ and the scale is fixed ($p_T = 0$) so x_1 and x_2 are known at each y – compare red line with circles on the left

Factorization is not automatic at NLO because process is $2 \to 2\,[(c\overline{c}) + g/q/\overline{q}]$ and the additional parton makes the correspondence between x_1, x_2 and y inexact, even at fixed rapidity – agreement is good, nevertheless

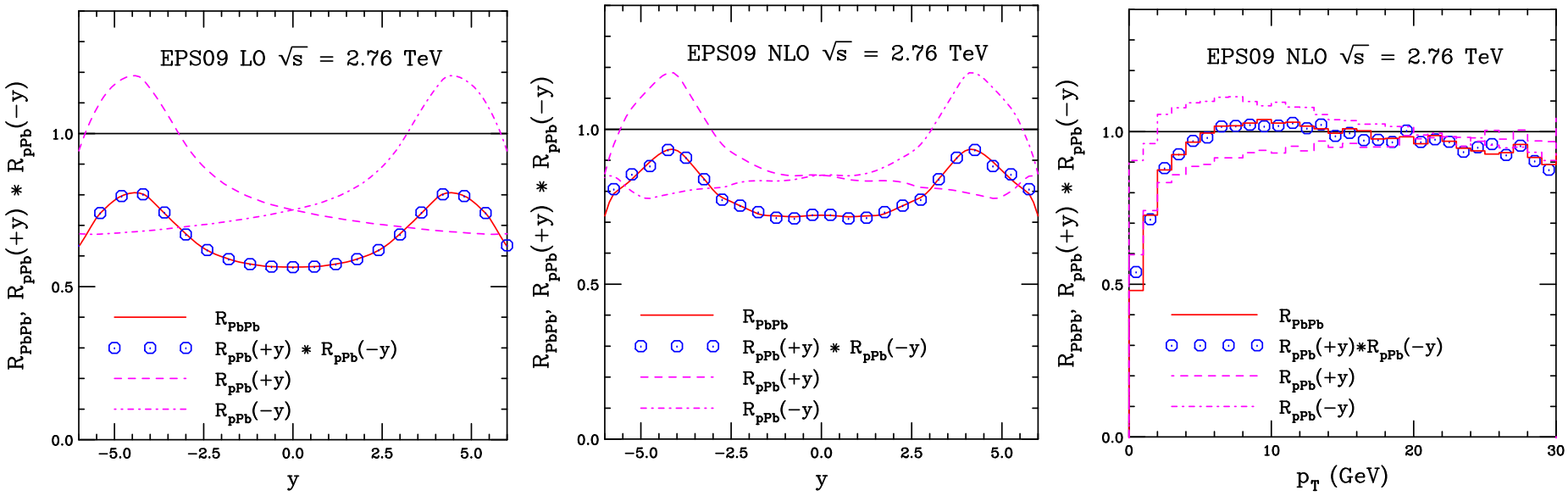

Figure 18: **The R_{AA} (red) ratio is compared to the product $R_{pA}(+y) \times R_{pA}(-y)$ (points) along with the individual pA ratios at forward (dashed) and backward (dot-dashed) rapidity. Results are compared for the rapidity distributions at LO (left) and NLO (middle) as well as for the p_T dependence at NLO (right).**

Factorization of R_{AA} into $R_{pA}(+y) \times R_{pA}(-y)$? Υ

Agreement also good for Υ production even though there is somewhat more scatter at high p_T

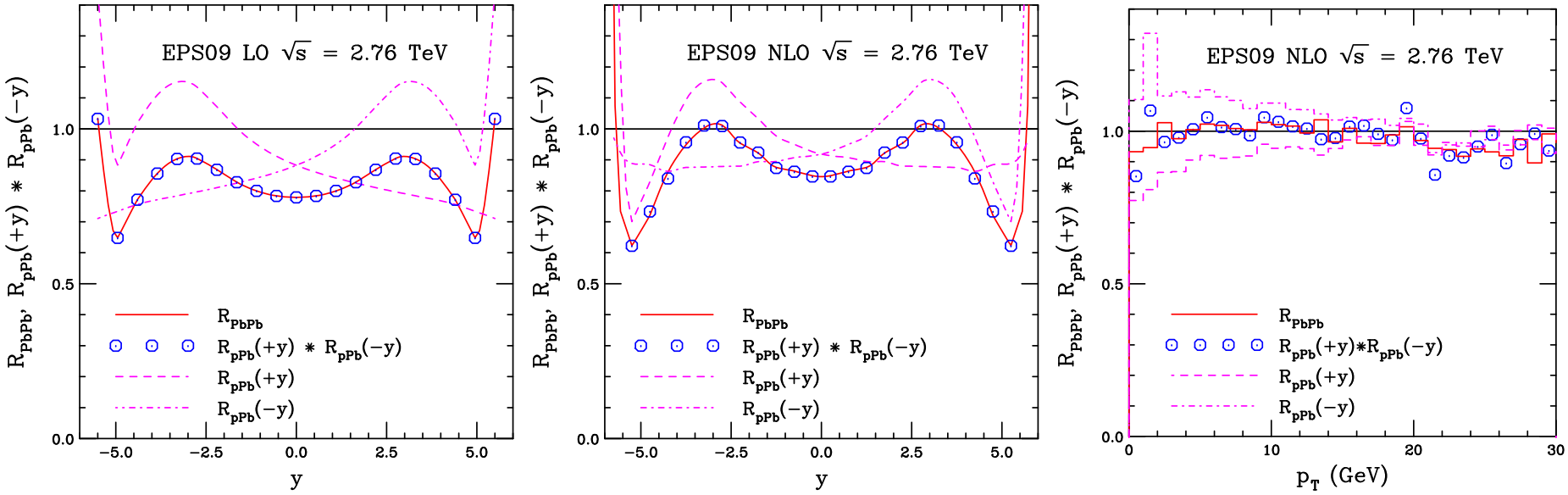

Figure 19: **The R_{AA} (red) ratio is compared to the product $R_{pA}(+y) \times R_{pA}(-y)$ (points) along with the individual pA ratios at forward (dashed) and backward (dot-dashed) rapidity. Results are compared for the rapidity distributions at LO (left) and NLO (middle) as well as for the p_T dependence at NLO (right).**

Summary

- **Fitting the scale parameters to the total $Q\overline{Q}$ cross section data significantly reduces the uncertainties on open heavy flavor and quarkonium production**
- **Differences in LO and NLO results for EPS09 on J/ψ production illustrates the fact that gluon nPDF is still not very well constrained, although, given the approximate concordance of the nDS results, the EPS09 discrepancy may be due to the choice of CTEQ6 proton PDFs**
- **LHC p+Pb hadroproduction data could be taken into global analyses in the future but many caveats on medium effects, *e.g.* initial and/or final state energy loss, production mechanism, saturation effects – while the $R_{p\mathrm{Pb}}$ results, both as a function of p_T and y, look good, the R_{FB} results are not as good: pp data at 5 TeV are required**